



2007-12-21

Incorporating Grain Size Effects in Taylor Crystal Plasticity

Bradley S. Fromm

Brigham Young University - Provo

Follow this and additional works at: <https://scholarsarchive.byu.edu/etd>



Part of the [Mechanical Engineering Commons](#)

BYU ScholarsArchive Citation

Fromm, Bradley S., "Incorporating Grain Size Effects in Taylor Crystal Plasticity" (2007). *All Theses and Dissertations*. 1275.
<https://scholarsarchive.byu.edu/etd/1275>

This Thesis is brought to you for free and open access by BYU ScholarsArchive. It has been accepted for inclusion in All Theses and Dissertations by an authorized administrator of BYU ScholarsArchive. For more information, please contact scholarsarchive@byu.edu, ellen_amatangelo@byu.edu.

INCORPORATING GRAIN SIZE EFFECTS IN
TAYLOR CRYSTAL PLASTICITY

by

Bradley S. Fromm

A thesis submitted to the faculty of

Brigham Young University

in partial fulfillment of the requirements for the degree of

Master of Science

Department of Mechanical Engineering

Brigham Young University

April 2008

Copyright © 2008 Bradley S. Fromm

All Right Reserved

BRIGHAM YOUNG UNIVERSITY

GRADUATE COMMITTEE APPROVAL

of a thesis submitted by

Bradley S. Fromm

This thesis has been read by each member of the following graduate committee and by majority vote has been found to be satisfactory.

Date

Brent L. Adams, Chair

Date

Brian D. Jensen

Date

Michael P. Miles

BRIGHAM YOUNG UNIVERSITY

As chair of the candidate's graduate committee, I have read the thesis of Bradley S. Fromm in its final form and have found that (1) its format, citations, and bibliographical style are consistent and acceptable and fulfill university and department style requirements; (2) its illustrative materials including figures, tables, and charts are in place; and (3) the final manuscript is satisfactory to the graduate committee and is ready for submission to the university library.

Date

Brent L. Adams
Chair, Graduate Committee

Accepted for the Department

Matthew R. Jones
Graduate Coordinator

Accepted for the College

Alan R. Parkinson
Dean, Ira A. Fulton College of Engineering
and Technology

ABSTRACT

INCORPORATING GRAIN SIZE EFFECTS IN TAYLOR CRYSTAL PLASTICITY

Bradley S. Fromm

Department of Mechanical Engineering

Master of Science

A method to incorporate grain size effects into crystal plasticity is presented. The classical Hall-Petch equation inaccurately predicts the macroscopic yield strength for materials with non-equiaxed grains or materials that contain unequal grain size distributions. These deficiencies can be overcome by incorporating both grain size and orientation characteristics into crystal plasticity theory. Homogenization relationships based on a viscoplastic Taylor-like approach are introduced along with a new function, the grain size and orientation distribution function (GSODF). Estimates of the GSODF for high purity α -titanium are recovered through orientation imaging microscopy coupled with the chord length distribution. A comparison between the new method and the traditional viscoplastic Taylor approach is made by evaluating yield surface plots.

ACKNOWLEDGMENTS

This project was completed due to the help and encouragement of many people. I am grateful for the patient guidance offered by my advisor, Professor Brent L. Adams, along with the help and encouragement of my committee, Professor Brian D. Jensen and Professor Michael P. Miles. I appreciate the continuous help from members of my research group, especially Sadegh Ahmadi who spent countless hours debugging computer code. I express appreciation to Professor Surya R. Kalidindi's research group, particularly Marko Knezevic, for providing the titanium material, sharing their crystal plasticity code, helping to calibrate the model, and performing compression testing. I would also like to express my love and appreciation to my wife Brenda and our children for supporting me and believing in me during a very difficult time, as well as our extended families who contributed many prayers in our behalf. Finally, I would like to acknowledge the Army Research Office and especially Dr. David M. Stepp for providing funding for this research

TABLE OF CONTENTS

1	Introduction	1
2	Hall-Petch Relationships	3
	2.1 Macroscopic Hall-Petch equation.....	3
	2.2 Microscale Hall-Petch correlation	3
	2.3 New mesoscale Hall-Petch relationship	4
3	Taylor viscoplastic model for high purity α-titanium	7
	3.1 Power law equation.....	7
	3.2 Yield strength calculations.....	8
4	New grain size differentiated Taylor-type model	9
	4.1 Modified power law equations	9
	4.2 Selected approach to yield strength calculation.....	9
	4.3 Grain size and orientation distribution function	10
	4.4 New grain size dependent Taylor factor	11
	4.5 Chord length distribution	12
5	Experimental methods on high purity α-titanium	15
	5.1 High purity α -titanium background information	15
	5.2 Oblique sectioning and sample preparation.....	16
	5.3 OIM analysis and results.....	17
	5.4 Chord length distribution plots	20
	5.5 Comparison between OIM and CLDF grain size statistics.....	20

5.6	Chord length spacing sensitivity.....	21
5.7	ODF and grain statistics plots.....	22
5.8	True stress – true strain plots.....	23
6	Calibration and evaluation of model.....	25
6.1	Calculation of reference shear stresses.....	25
6.2	Numerical challenges.....	25
6.3	Database approach.....	26
6.4	Discretization scheme.....	28
7	Discussion of Results.....	29
7.1	Deviatoric stress subspace.....	29
7.2	Yield surface plots.....	30
7.3	Effect of numerical methods on yield surfaces.....	31
8	Conclusions.....	35
	References.....	37

LIST OF TABLES

Table 5.1: Section plane normal spherical coordinates and associated Euler angles	16
Table 5.2: Grain statistics obtained from analysis of OIM data	19
Table 5.3: Comparison of grain size statistics calculated from OIM and CLDF	21
Table 6.1: Mesoscale Hall-Petch parameters.....	26

LIST OF FIGURES

Figure 1.1:	Deformed and partially recrystallized iron aluminide illustrating non-equiaxed grain shapes and unequal grain size distributions often found in engineered materials (image courtesy of Oxford Instruments).....	2
Figure 5.1:	Pole figure plots illustrating texture of heat treated α -titanium plate with c-axis of grains distributed around ND direction.....	15
Figure 5.2:	(a) Sphere of directions representing surface normal directions for oblique section cuts, (b) Rendering of titanium plate with 13 section cuts removed and ND, RD, and TD directions defined.....	17
Figure 5.3:	Inverse pole figure maps and pole figures for section 1 (a), section 2 (b), and section 3 (c).....	18
Figure 5.4:	Grains size distribution from OIM analysis	19
Figure 5.5:	Chord length distribution plot	20
Figure 5.6:	CLDF chord spacing error plot	22
Figure 5.7:	Orientation distribution plots, maximum grain size, mean grain size, and standard deviation plots are presented for several cross sections of the fundamental zone	23
Figure 5.8:	True stress - true strain curves from uniaxial and plane strain compression testing.....	24
Figure 6.1:	Discretized HCP fundamental zone shown for 10 degree bin sizes.....	28
Figure 7.1:	Deviatoric stress subspace plot for high purity α -titanium (all units are in MPa).....	29
Figure 7.2:	Pi-section yield surface comparing Von-Mises yield surface in red, traditional Taylor model in black, and the new grain size dependent model in blue (all units are in MPa).....	31
Figure 7.3:	Effect of grain size bins on size of yield surface where the black curve was calculated with a single grain size bin, the green curve incremented	

grains size into 10 segments, and the blue curve represents the curve
calculated with 40 grain size bins (all units are MPa)32

1 Introduction

Predicting the yield strength of engineered materials based on their grain size is common practice within the materials community. During the early 1950's, E.O. Hall and N.J. Petch independently established what is known as the Hall-Petch relationship [1-2]. Through experimentation, they discovered that the macroscopic yield strength of a material is proportional to the inverse square root of the average grain size. This robust relationship has been documented for many materials [3]. It indicates that yield strength can be increased by simply reducing grain size. However, as represented in Figure 1.1, it does not hold true for materials with non-equiaxed grains or materials that contain unequal grain size distributions. The relationship has also been shown to breakdown for ultrafine grained materials [4]. A further weakness to the relationship is that it does not take into account the grain orientation or crystal anisotropy within the microstructure.

Similarly, crystal plasticity theory dates back to 1938 when G.I. Taylor postulated his uniform strain model in order to predict yield strength [5]. This method calculates the stresses in individual grains of a material by resolving the strain rate for each grain in terms of slip rates on individual slip systems. The microscopic stress of each grain is then volume averaged to obtain an upper-bound estimate for the macroscopic yield strength. Although this method takes grain orientation into account and is valid for non-

equiaxed and anisotropic materials, it does not distinguish the effect of local grain size on the local yield properties.



Figure 1.1: Deformed and partially recrystallized iron aluminide illustrating non-equiaxed grain shapes and unequal grain size distributions often found in engineered materials (image courtesy of Oxford Instruments)

The purpose of the research described in this paper is to extend crystal plasticity theory to incorporate both grain orientation and grain size effects into the model, thus overcoming current deficiencies in yield strength calculations. A new approach that incorporates a Hall-Petch type relationship into a rigid-viscoplastic model is described. This new methodology is then implemented for a high purity α -titanium material and a comparison is made between the old and new methods to determine the extent to which grain size affects the mechanical strength of the material.

2 Hall-Petch Relationships

2.1 Macroscopic Hall-Petch equation

Relation (2.1) is the well known Hall-Petch equation where σ_y is the macroscopic yield strength, σ_0 is the stress required to initiate dislocation movement (incorporating all strengthening effects except the grain size effect), K is the Hall-Petch slope, and \bar{D} is the average grain size of the material

$$\sigma_y = \sigma_0 + \frac{K}{\sqrt{\bar{D}}} \quad (2.1)$$

This empirical relationship has been established for numerous metal alloys, including high purity α -titanium, which is studied in this paper. Values for both σ_0 and K are obtained through mechanical testing. Values of 0.53 and 0.671 MN/m^{3/2} for the slope were found in the literature for α -titanium [6-7]. These large values of slope indicate that grain size effects are important when modeling the yield stress of titanium.

2.2 Microscale Hall-Petch correlation

The macroscopic Hall-Petch relationship has been successfully extended to the microscale by studying slip transmission across grain boundaries [8-9]. In this method,

nano-indentation is employed to determine the applied shear stress, τ_a , necessary to force dislocations across a grain boundary according to

$$\tau_a = \tau_0 + \frac{k}{\sqrt{D}}, \quad (2.2)$$

where τ_0 is the intrinsic frictional shear stress and \bar{D} is the average grain size, as delineated by the distance between the indenter and the adjacent grain boundary. Further, $k = 2m^{-1}\tau_c\sqrt{r}$ is the equation for the slope where m represents the misorientation between the slip systems on each side of the grain boundary, τ_c is the critical shear stress required to initiate slip across the boundary, and r is the distance to the dislocation source in the neighboring grain.

2.3 New mesoscale Hall-Petch relationship

The general nature of the Hall-Petch relationships suggests the possibility of extending them to the concept of a critical resolved shear stress in rate-insensitive plasticity, and to the reference shear stress in viscoplasticity theory. Although Relation (2.2) appears simple at first, implementation is problematical due to the grain boundary character dependence of both τ^* and r within the slope equation. Further, homogenization procedures used to connect the two relationships are not well understood.

A new relationship is necessary to integrate grain size information into the viscoplasticity model,

$$\tau^{*(S)} = \tau_0^{(S)} + \frac{k^{*(S)}}{\sqrt{D}}, \quad (2.3)$$

Where $\tau^{*(S)}$ is the reference shear stress or slip resistance and $k^{*(S)}$ is the Hall-Petch like slope, resolved on each slip system of the model. It should be noted that D , which has been substituted in the place of \bar{D} , is no longer the average grain size of the bulk material but the actual grain size for each individual grain within the material; this is allowed to vary within the crystal plasticity model.

3 Taylor viscoplastic model for high purity α -titanium

3.1 Power law equation

The crystal plasticity model utilized in this research is the standard power-law viscoplasticity approach of Asaro and Needleman [10] as implemented by Kalidindi et al [11-14]. The power law,

$$\dot{\epsilon}_{ij} = \sum_{s=1}^S \dot{\gamma}^{(s)} \mu_{ij}^{(s)}, \quad (3.1)$$

relates strain rates $\dot{\epsilon}_{ij}$ in terms of slip rates $\dot{\gamma}$ on individual slip systems S , with the geometry of the slip system defined by the geometric slip tensor μ_{ij} , according to

$$\mu_{ij}^{(s)} = \frac{1}{2} \left(\hat{b}_i^{(s)} \hat{n}_j^{(s)} + \hat{b}_j^{(s)} \hat{n}_i^{(s)} \right). \quad (3.2)$$

Here $\hat{b}^{(s)}$ and $\hat{n}^{(s)}$ are defined as the unit slip and normal directions respectively. By assuming isotropic hardening, the slip rates can be expressed as:

$$\dot{\gamma}^{(s)} = \dot{\gamma}_0 \left| \frac{\tau^{(s)}}{\tau_R^{(s)}} \right|^{\frac{1}{m}} \text{sign}(\tau^{(s)}), \quad (3.3)$$

where $\tau^{(s)} = \sigma'_{ij} \mu_{ij}^{(s)}$ is the resolved shear stress associated with each slip system, $\tau_R^{(s)}$ is the slip resistance, m is the strain rate sensitivity factor, and σ'_{ij} is the deviatoric component of the local Cauchy stress.

3.2 Yield strength calculations

The power law equation can be re-written in terms of the viscoplastic compliance [15], M , as

$$\dot{\varepsilon}_{ij} = M_{ijkl} \sigma'_{kl}. \quad (3.4)$$

By applying the Taylor assumption wherein the local and macroscopic strain rates are equal [5], Equation (3.4) can be solved for the local stress, and volume averaged for each grain in the polycrystal to obtain

$$\bar{\sigma}'_{kl} = \langle \sigma'_{kl} \rangle = \frac{1}{V} \iiint_V \sigma'_{kl} dV. \quad (3.5)$$

Relation (3.5) estimates the macroscopic deviatoric stress $\bar{\sigma}'_{kl}$ in a sample that occupies a region of volume V comprising a representative volume element of the bulk polycrystalline sample. Instead of directly volume averaging the local stresses to obtain the macroscopic yield strength, the classical approach can be taken – this requires the Taylor factor. The deviatoric stress can be expressed in terms of the local Taylor factor, m_{kl} , to obtain the relationship

$$\sigma'_{kl} = m_{kl} \tau_R \text{ or } m_{kl} = \frac{\sigma'_{kl}}{\tau_R}. \quad (3.6)$$

The Taylor factor expresses the efficiency by which deformation is affected by the lattice orientation of crystallographic slip and is thus a function of orientation, strain rate sensitivity parameter, and slip resistance. By simply volume averaging the local Taylor factor and scaling it by the reference shear stress, an alternative means of calculating the average macroscopic deviatoric stress can be expressed as

$$\bar{\sigma}'_{kl} = \langle m_{kl} \rangle \tau_R^{(S)}. \quad (3.7)$$

4 New grain size differentiated Taylor-type model

4.1 Modified power law equations

Equations (3.1)-(3.7) represent the traditional Taylor-like viscoplastic approach to crystal plasticity. They are not grain size dependent and thus require modification. By inserting $\tau^{*(s)}$ from the newly defined mesoscale Hall-Petch Relation (2.3) into Equation (3.3), the slip rate equation becomes

$$\tilde{\gamma}^{(s)} = \dot{\gamma}_0 \left| \frac{\tau^{(s)}}{\tau^{*(s)}} \right|^{\frac{1}{m}} \text{sign}(\tau^{(s)}). \quad (4.1)$$

A new power law relationship can now be formulated that contains the grain size differentiated slip rate equation as represented in Equation (4.2).

$$\tilde{\varepsilon}_{ij} = \sum_{s=1}^S \tilde{\gamma}^{(s)} \mu_{ij}^{(s)} \quad (4.2)$$

Thus the power law relationships have become modified to allow grain size to vary for each individual grain in the Taylor-type viscoplasticity model.

4.2 Selected approach to yield strength calculation

Just as the power law was modified to allow grain size to vary, it is necessary to adjust the macroscopic yield strength to elucidate the grain size effect within the Taylor model as defined in the following relation:

$$\bar{\sigma}'_{kl} = \langle \tilde{m}_{kl} \rangle \bar{\tau}_0. \quad (4.3)$$

Although Equation (4.3) appears similar to Relation (3.7), it differs in several ways. First, the slip resistance has been replaced by $\bar{\tau}_0 = \frac{1}{3}(\tau_0^{bas} + \tau_0^{pris} + \tau_0^{pyr})$ that represents the average values of intrinsic frictional shear stress in the basal, prismatic, and pyramidal slip systems for hexagonal titanium. A further difference is the introduction of a new variable, \tilde{m}_{kl} , that is related to the familiar Taylor Factor in Equation (3.7), but has been adjusted for grain size. Thus \tilde{m}_{kl} is not only a function of the crystallographic orientation, the ratio of intrinsic frictional shear stresses, and the strain rate sensitivity parameter, but also of grain size. Moreover, this new variable can be calculated from the local Cauchy stress as demonstrated in Equation (4.4).

$$\sigma'_{kl} = \tilde{m}_{kl} \bar{\tau}_0 \text{ or } \tilde{m}_{kl} = \frac{\sigma'_{kl}}{\bar{\tau}_0} \quad (4.4)$$

4.3 Grain size and orientation distribution function

It is proposed that a new distribution function, called the *grain size and orientation distribution function* (GSODF), be defined so that the Taylor factor can be evaluated explicitly. This function is similar to the orientation distribution function (ODF) in that it contains volume fractions of grain orientation occurrences, but differs in that it also includes the grain size. It is expressed as

$$f(g, D) dg dD = \frac{dV}{V}, \quad (4.5)$$

and is defined as the probability density of finding an occurrence of grain size D with an orientation g inside a single phase polycrystalline material sample. If the GSODF is integrated over the full range of grain size, it returns the familiar ODF:

$$\int_0^{D_{\max}} f(g, D) dD = f(g) . \quad (4.6)$$

On the other hand, if the GSODF is integrated over the full range of possible lattice orientation (i.e., the fundamental zone, FZ), then the overall grain size distribution of the microstructure $\overline{f(D)}$ is recovered:

$$\iiint_{FZ} f(g, D) dg = \overline{f(D)} . \quad (4.7)$$

Lastly, the following normalization condition must hold:

$$\int_0^{D_{\max}} \iiint_{FZ} f(g, D) dg dD = 1 . \quad (4.8)$$

4.4 New grain size dependent Taylor factor

Next, a new factor similar to the macroscopic Taylor factor is defined by integrating the local grain size dependent Taylor factor with the GSODF to yield:

$$\langle \tilde{m}_{kl}(g, D) \rangle = \int_0^{D_{\max}} \iiint_{FZ} f(g, D) \tilde{m}_{kl}(g, D) dg dD . \quad (4.9)$$

Whereas the original Taylor factor expresses the efficiency by which deformation is affected by the lattice orientation of crystallographic slip, this new grain size dependent Taylor factor expresses the same efficiency as a function of both lattice orientation and grain size. By inserting Relation (4.9) into Equation (4.3), the macroscopic yield strength can be evaluated as both a function of orientation and grain size.

4.5 Chord length distribution

A second distribution, called the Chord Length Distribution function (CLDF) [16-17], must be introduced to recover the GSODF experimentally. The CLDF is defined as the probability that a random chord traversing a grain will sample a grain of orientation g with a chord length of $D \pm dD/2$ within invariant orientation measure dg and along an infinite line containing the vector $\vec{c}^{(s)}$.

$$p(g, D | \vec{c}^{(s)}) dg dD. \quad (4.10)$$

The superscript s is used to indicate that we have chosen to resolve chord lengths in directions that correspond to the intersection of slip planes with the metallographic section plane. The direction of the chord, $\vec{c}^{(s)}$, for each slip system is obtained by taking the cross product between the section plane normal \hat{N} and the slip plane normal $\hat{n}^{(s)}$,

$$\vec{c}^{(s)} = \hat{N} \times \hat{n}^{(s)}. \quad (4.11)$$

Because the chords traverse a grain from one side to the other, they are closely related to the grain's size, D . Hereafter, we shall make no distinction between the term “chord length” and the term “grain size.” Additionally, because multiple slip systems within each grain are sampled, a distribution of chord lengths will result for each grain. Thus, even a single grain will present a range of grain sizes that can be utilized for the purpose of distinguishing grain size effects within the methodology of this paper.

The reader will note the similarity between the GSODF and the CLDF. In fact, they are essentially the same function for equiaxed grain structures. However, for microstructures with peculiar grain shapes, differences would be expected between the

two functions. The normalization of the CLDF is obvious from its definition:

$$\int_0^{D_{\max}} \iiint_{FZ} p(g, D | \bar{c}^{(S)}) dg dD = 1. \quad (4.12)$$

Clearly, the CLDF is very similar to the GSODF that is desired to modify Taylor viscoplasticity. In fact, the CLDF is essentially the GSOD, but specific to each slip system. This is an important difference since individual slip systems (such as $\{10\bar{1}0\}\langle 11\bar{2}0\rangle$ versus $\{10\bar{1}1\}\langle 11\bar{2}3\rangle$ in some hexagonal materials) may sample grain size differently. This is especially true for grains of unusual morphologies which contain crystallographic orientations that can be linked to processes such as solidification or grain growth. For that which follows in this paper, we shall not distinguish local grain size among the differing slip systems, but only the variation of grain size with grain orientation. In this case the GSODF will be expressed in terms of the CLDF as an average over the total number of slip systems, S :

$$f(g, D) = \frac{1}{S} \sum_{s=1}^S p(g, D | \bar{c}^{(S)}). \quad (4.13)$$

Consequently, the output of the GSODF contains for any given orientation, g , a range of grain sizes, and this distribution is affected not only by the distribution of sizes of grains of a particular class, but also by the specific chord length distribution of that class.

5 Experimental methods on high purity α -titanium

5.1 High purity α -titanium background information

The high purity α titanium material used in this study was supplied by the Alta Group of Johnson Matthey Electronics, Inc. (Spokane, WA). The received plate was 99.9998% pure and measured 352 mm in diameter by 12 mm in thickness. The material was heat treated at 530° C for one hour and water quenched to produce a recrystallized grain structure with an average grain size of 11 μm . As detailed in previous research [6,7,11,13,18] and shown in the [0 0 0 1] pole figure of Figure 2, the material exhibits a strong fiber texture with the c -axes of the grains distributed uniformly within 20-35° of the plate normal (ND) following heat treatment.

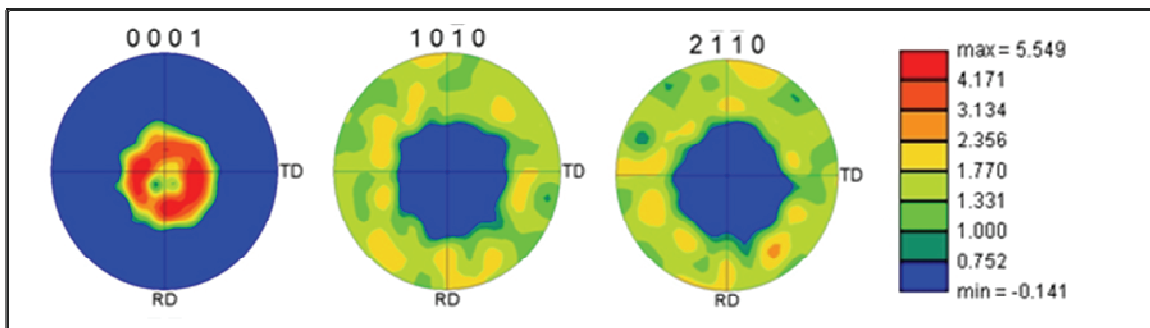


Figure 5.1: Pole figure plots illustrating texture of heat treated α -titanium plate with c -axis of grains distributed around ND direction

5.2 Oblique sectioning and sample preparation

In order to recover the CLDF and GSODF of the high purity α titanium in a statistically-unbiased way, an oblique sectioning technique was employed. The sphere of directions in Figure 5.2(a) represents the surface normal directions for the 13 oblique section cuts along with their inverses. The points circled in black are found on the front of the sphere, while the points circled in gray are located on the back side of the sphere. Figure 5.2(b) is a rendering of the titanium sample with the section cuts removed and a coordinate system that defines the ND, TD, and RD directions of the sample. The spherical coordinates for each section cut normal along with their associated Euler angles are tabulated in Table 5.1.

Table 5.1: Section plane normal spherical coordinates and associated Euler angles

Section #	Polar Angle (α)	Azimuth Angle (β)	Euler Angle (ϕ_1)	Euler Angle (PHI)	Euler Angle (ϕ_2)
1	0°	0°	0°	0°	270°
2	45°	0°	90°	45°	270°
3	90°	0°	90°	90°	270°
4	135°	0°	90°	135°	270°
5	45°	45°	135°	45°	270°
6	90°	45°	135°	90°	270°
7	135°	45°	135°	135°	270°
8	45°	90°	180°	45°	270°
9	90°	90°	180°	90°	270°
10	135°	90°	180°	135°	270°
11	45°	135°	225°	45°	270°
12	90°	135°	225°	90°	270°
13	135°	135°	225°	135°	270°

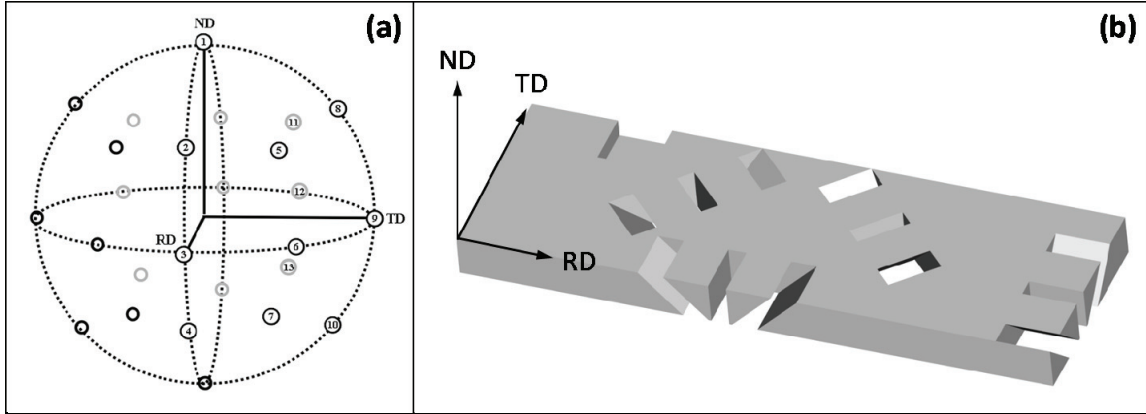


Figure 5.2: (a) Sphere of directions representing surface normal directions for oblique section cuts, (b) Rendering of titanium plate with 13 section cuts removed and ND, RD, and TD directions defined

The samples were electrical discharge machined from the heat treated titanium plate and carefully polished to remove deformation incurred from the sectioning process. This included successive polishing from an initial abrasive of 320 grit SiC to a final polish with a 0.05 μm γ -alumina suspension. Next, the samples were immersed in an agitated solution of Keller's reagent (2 ml HF, 3 ml HCl, 5 ml HNO₃, and 190 ml distilled water) for 45 seconds to remove any remaining oxides and surface deformation caused by polishing.

5.3 OIM analysis and results

Orientation imaging microscopy (OIM) was performed on a Philips XL-30SFEG scanning electron microscope for each of the 13 samples in order to obtain the orientation and grain size statistics. A hexagonal grid with a 1 μm step size yielded 208,247 scan points within the 300 μm x 600 μm scan window. Inverse pole figure maps for oblique sections 1, 2 and 3 are shown in Figure 5.3 along with their corresponding $[0\ 0\ 0\ 1]$ pole figures.

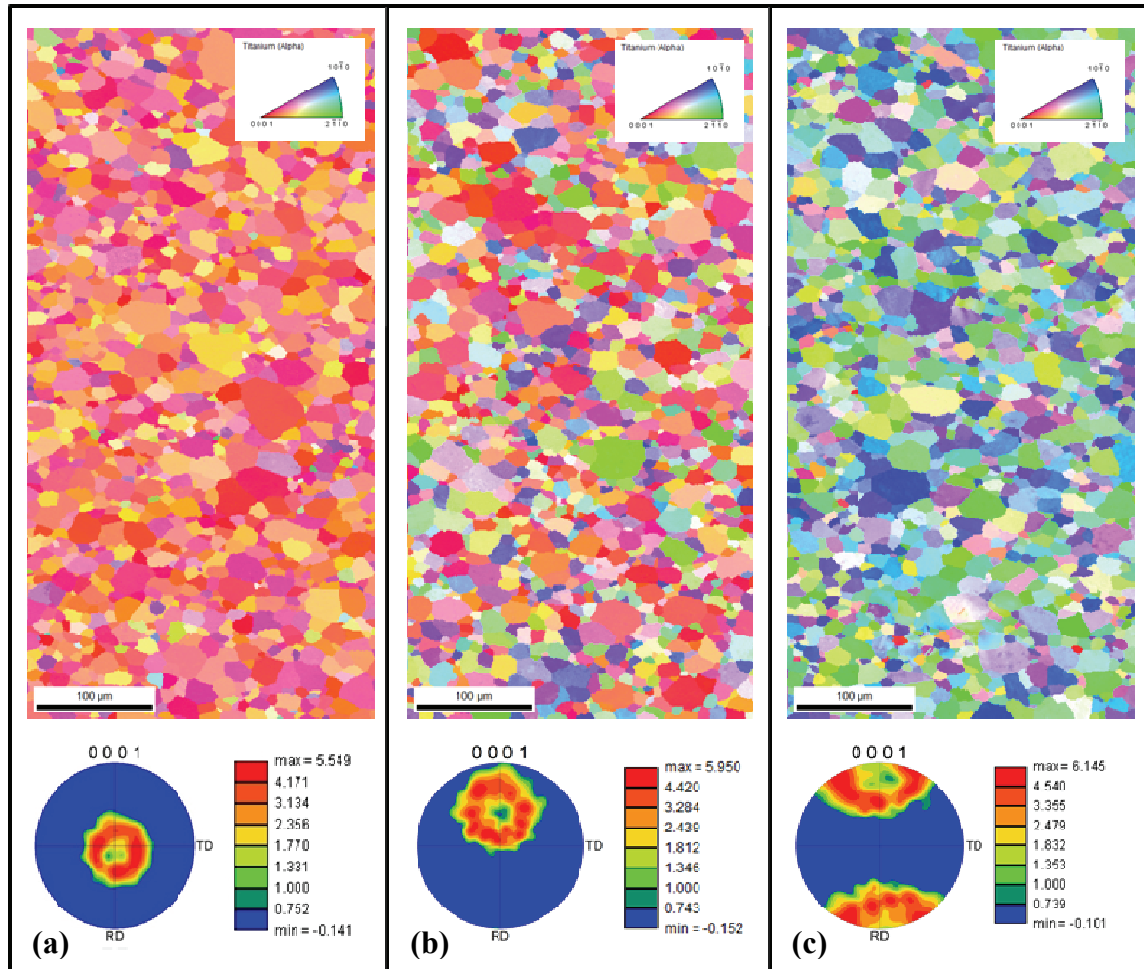


Figure 5.3: Inverse pole figure maps and pole figures for section 1 (a), section 2 (b), and section 3 (c)

A summary of the maximum, minimum, and average grain size, as well as standard grain size deviation can be found in Table 5.2 for each of the 13 oblique sections. The α -titanium material in this study had an overall average grains size of 11.09 with a standard deviation of 5.64 μm , as measured by the equivalent diameter method in OIM. A total of 19,642 grains were resolved but since edge grains were excluded from the analysis, only 17,437 were included in the statistics. A combined grain size distribution plot for all 13 sections is shown in Figure 5.4.

Table 5.2: Grain statistics obtained from analysis of OIM data

Section Number	Number of Grains	Number of Non-Edge Grains	Minimum Diameter (μm)	Maximum Diameter (μm)	Average Grain Size (μm)	Standard Deviation (μm)
1	1540	1352	3.321	50.655	10.960	5.590
2	1517	1341	3.321	42.304	11.068	5.477
3	1524	1352	3.321	39.820	11.033	5.642
4	1496	1328	3.321	44.153	11.025	5.771
5	1700	1525	3.321	44.166	10.426	5.270
6	1581	1411	3.321	37.392	10.868	5.512
7	1280	1122	3.483	46.215	12.028	6.084
8	1800	1614	3.321	35.377	10.254	4.906
9	1535	1364	3.321	49.231	11.019	5.446
10	1499	1308	3.321	38.839	11.195	5.649
11	1646	1480	3.321	36.315	10.669	5.133
12	1262	1105	3.321	50.184	11.952	6.435
13	1292	1135	3.321	51.827	11.720	6.430
	19,672	17,437	3.321	51.827	11.094	5.642

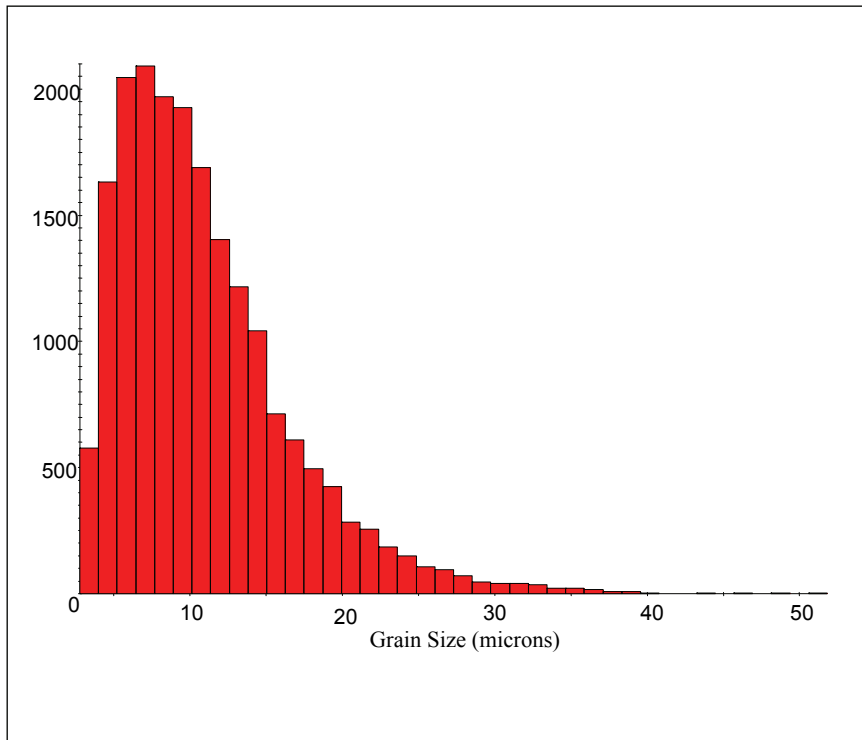


Figure 5.4: Grains size distribution from OIM analysis

5.4 Chord length distribution plots

A chord length distribution plot is presented in Figure 5.5 for three of the primary hexagonal slip systems of titanium. In this way the CLDF was used to calculate the average grain size for each of the 17,437 grains examined with orientation imaging microscopy. However, the complete subset of primary slip systems totaling 18 were sampled and then averaged to obtain the grain size values input into the Taylor model.

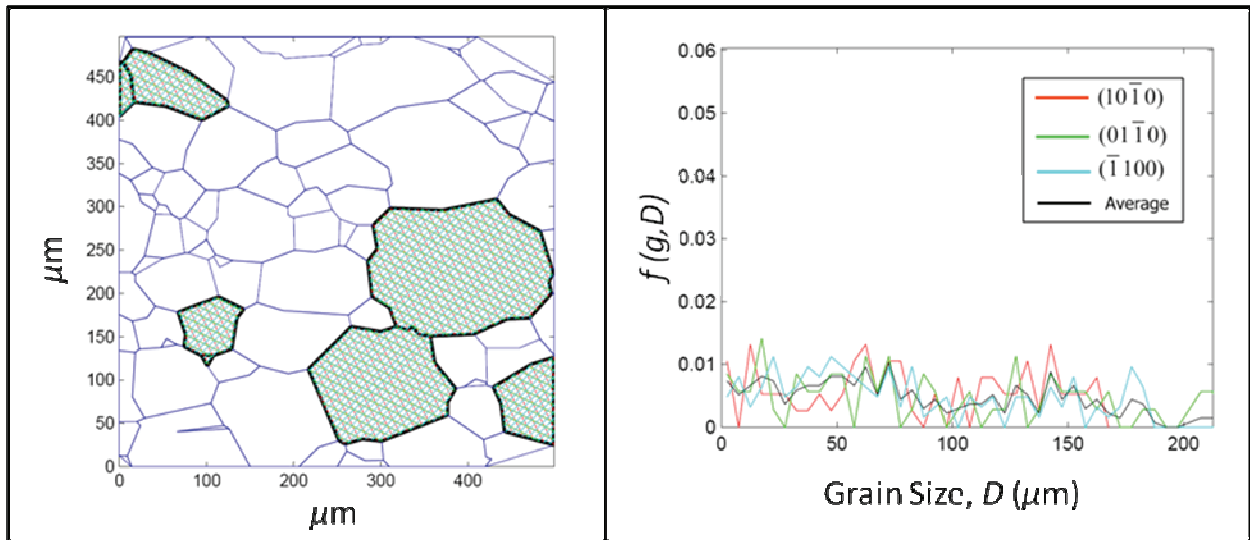


Figure 5.5: Chord length distribution plot

5.5 Comparison between OIM and CLDF grain size statistics

The overall average grain size for the α -titanium material as calculated by the CLDF method was $7.72 \mu\text{m}$ with a standard deviation of $4.35 \mu\text{m}$. This compares nicely to the OIM value of $11.09 \pm 5.64 \mu\text{m}$. The difference between the two methods is due to the grain geometry and how grain size is calculated. If the two methods returned the same results, we would assume the grains were equiaxed since the OIM approach calculates the equivalent grain diameter from the area of the grain. Because they are

different, we can assume that the grains are slightly non spherical. This was verified by calculating the average grain's shape within OIM. The results show that the grains are elongated with an average major diameter of 7.24 μm vs. a minor diameter of 5.24 μm using the least squares method. Table 5.3 summarizes the important grain size statistics as calculated by both methods.

Table 5.3: Comparison of grain size statistics calculated from OIM and CLDF

Grain Size Statistics	OIM	CLDF
Minimum Grain size (μm)	3.321	0.335
Maximum Grain size (μm)	51.827	38.126
Average Grain Size (μm)	11.094	7.715
Standard Deviation (μm)	5.642	4.346

5.6 Chord length spacing sensitivity

In order to understand the influence spacing between chords plays in the chord length distribution function, a test was conducted to determine the average grain size for a 10 μm circle. For spacings between 0.01 μm and 1 μm the average chord length, \bar{L} was calculated and compared to the theoretical value of 7.8540, as obtained from the equation, $\bar{L} = \frac{\pi r}{2}$ [19]. The error plot shown in Figure 5.6 illustrates the need to carefully choose the spacing between chords. An average chord length of 7.8553 was calculated for a spacing of 0.01 μm which equates to an error of 0.016%. This value of spacing was used in our calculations to ensure precise measurements of the CLDF.

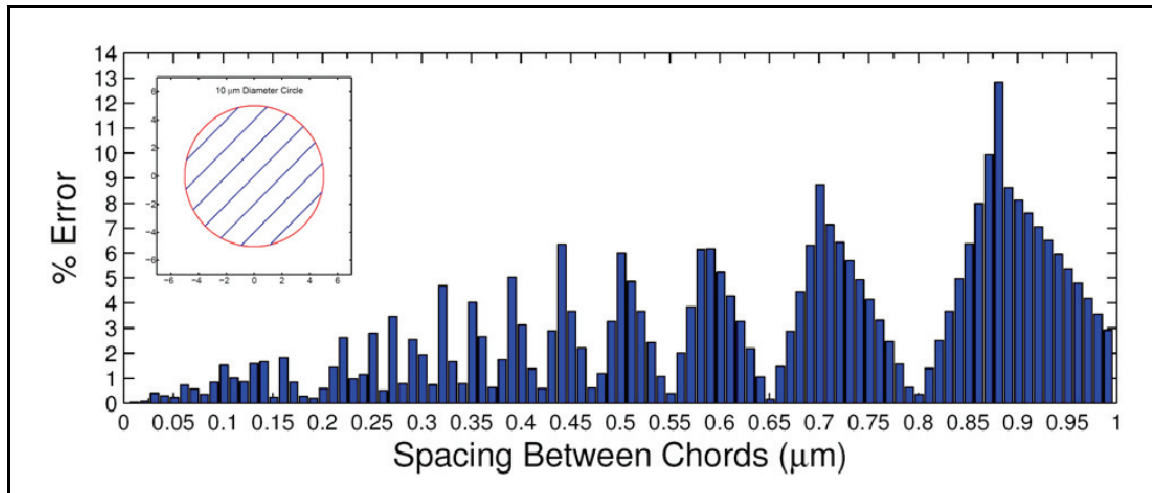


Figure 5.6: CLDF chord spacing error plot

5.7 ODF and grain statistics plots

Plots of the orientation distribution function, maximum grain size, mean grain size, and standard deviation calculated from the CLDF are found in Figure 5.7. Six cross sections were taken through the HCP fundamental zone at 0° , 60° , 120° , 180° , 240° , and 300° respectively. The peak intensity of the orientation distribution function was 6.36. The maximum grain size within any of the bins was 38.126 microns and the mean grain size for all bins was 7.7153 microns with a standard deviation of 3.76 microns.

It is noteworthy to mention that the variation of maximum grain size to average grain size is approximately 5 for α -titanium. This is substantial considering the grains were nearly equiaxed. Additionally, a comparison between the ODF plots and mean grain size plots demonstrate that crystal orientations and grain size do not necessarily correlate. Although a particular orientation is strongly present in a material, it is not guaranteed that the mean grain size distribution of that orientation is also large. We can conclude that the mechanical properties of α -titanium can vary substantially according to

its orientation distribution as well as its grain size distribution. Furthermore, titanium materials that contain acicular grain types or distribution with different grain sizes would result in an even larger change in variation that could substantially affect the overall strength of the material.

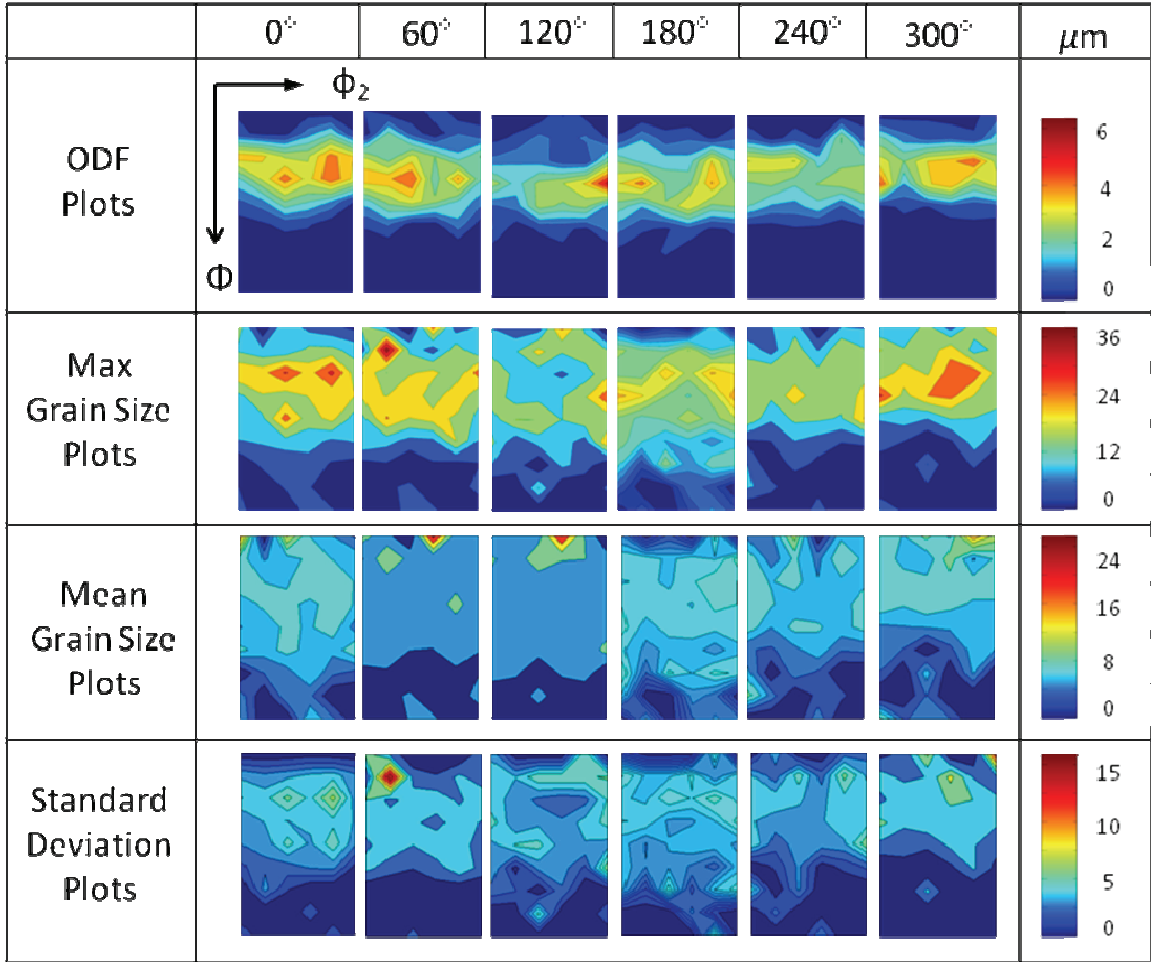


Figure 5.7: Orientation distribution plots, maximum grain size, mean grain size, and standard deviation plots are presented for several cross sections of the fundamental zone

5.8 True stress – true strain plots

In order to calibrate and verify the accuracy of the Taylor model predictions, uniaxial compression testing was performed for titanium test samples electrical discharge

machined from the plate in the RD, TD, and ND directions. The testing was performed at room temperature with a constant strain rate of 10^{-2} s^{-1} . During the test, Teflon sheets, high pressure grease, and regular lubrication were used to negate frictional effects. The raw load and displacement data was corrected for machine compliance before true stress –true strain curves were calculated. As plotted in Figure 5.8, the uniaxial compressive yield strength in the ND, RD, and TD directions was 352 MPa, 192 MPa, and 174 MPa respectively. Because the yield strength in the RD and TD directions is nearly the same, it was necessary to perform a fourth test to properly calibrate the model. A plane strain compression test in the ND direction was conducted and resulted in a yield strength of 199 MPa.

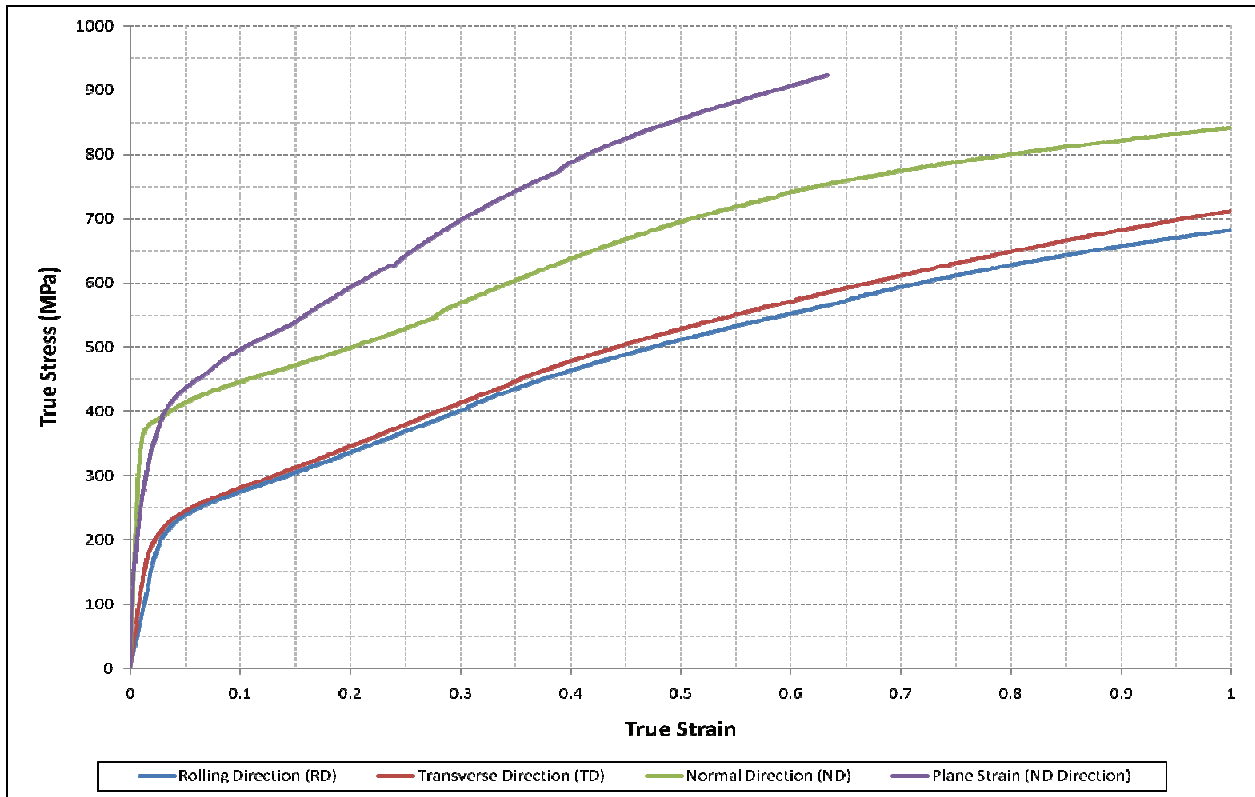


Figure 5.8: True stress - true strain curves from uniaxial and plane strain compression testing

6 Calibration and evaluation of model

6.1 Calculation of reference shear stresses

Reference shear stresses for the three primary slip families (basal, prismatic, and pyramidal) of hexagonal close pack titanium are necessary to calibrate the crystal plasticity model presented in this paper. These values were determined by curve-fitting the predicted yield strengths in simple deformation modes to the experimentally obtained curves shown in Figure 5.8 by trial and error until the predictions match the measured values. The values obtained through this process were 200 MPa, 10 MPa, and 120 MPa respectively for basal, prismatic, and pyramidal. Additionally, values of 57.1 MPa, 5.4 MPa, and 44.4 MPa for the basal, prismatic, and pyramidal intrinsic frictional shear stress were estimated based on the work of Churchman [20]. By substituting the abovementioned shear stresses along with the average value of grain size into Relation (2.3), we can calculate the values of the mesoscale Hall-Petch slope that are tabulated in Table 6.1.

6.2 Numerical challenges

Solving the Taylor viscoplastic equations for thousands of grains is computationally demanding. These five dimensional equations are known to converge poorly due to their stiff, non-linear nature. The situation becomes even more complex

when grain size effects are incorporated into the equations, as the calculations must be repeated for multiple grain sizes. A computationally efficient method is therefore needed that will eliminate the need to repeatedly solve the equations for every combination of grain orientation and size.

Table 6.1: Mesoscale Hall-Petch parameters

Slip System	$\tau^{*(S)}$ (MPa)	$\tau_0^{(S)}$ (MPa)	$k^{*(S)}$ (MN/m ^{3/2})
Basal	200	5.40	12.777
Prismatic	10	57.10	396.925
Pyramidal	120	44.40	209.999

6.3 Database approach

Knezevic et al [16] has developed a database approach where the necessary variables are computed only once and then stored for later retrieval. The strain rate equation can be written in terms of a single angular variable, θ , when expressed in its principal frame [17]. This is illustrated in Equation (6.1) where the reference value of strain rate, $\dot{\epsilon}_0$, has a value of 0.001 sec⁻¹. By working in the principal frame, only the diagonal terms of the strain rate space need to be sampled, and the time necessary to probe the entire five dimensional strain rate space is conserved.

The database is computed by tessellating θ into uniform intervals and solving for the deviatoric stresses at the centroid of each fundamental zone bin, which have also been tessellated into uniform bins. Because our model allows for variation of grain size, these

calculations must also be repeated for intervals of grain size uniformly distributed between zero and the maximum grain size.

$$\tilde{\dot{\epsilon}} = \dot{\epsilon}_0 \begin{bmatrix} \sqrt{\frac{2}{3}} \cos\left(\theta - \frac{\pi}{3}\right) & 0 & 0 \\ 0 & \sqrt{\frac{2}{3}} \cos\left(\theta + \frac{\pi}{3}\right) & 0 \\ 0 & 0 & -\sqrt{\frac{2}{3}} \cos(\theta) \end{bmatrix} \quad (6.1)$$

Discrete values of deviatoric stress in the principal frame, $\bar{\sigma}'_{kl}$, are thus stored for each value of theta between 0 and 2π . Nevertheless, we are interested in resolving the stresses in the sample frame, $\bar{\sigma}^S_{kl}$, of our titanium plate. Therefore, a method is required to enable the sample frame strain rate space to be uniformly sampled over all possible crystallographic orientations and θ increments to resolve the deviatoric stress in the sample frame. This is done by taking combinations of orientation and θ in the sample frame strain rate space, and decomposing them into their eigenvalues and eigenvectors. The eigenvalues give us the strain rate in the principal frame that corresponds to the sample frame strain rate that was input, whereas the eigenvectors give us a transformation matrix, ${}^{S \rightarrow P} \mathbf{g}$, which allows us to move back and forth between the principal and sample stresses. The database can thus be searched for the value of principal stress that corresponds to the principal strain rate obtained from the eigenvalues. Once the principal stress is known, the transformation matrix is used to convert it into the sample frame according to Equation (6.2).

$$[\bar{\sigma}^S] = \begin{bmatrix} {}^{S \rightarrow P} \mathbf{g} \end{bmatrix}^T [\bar{\sigma}^P] \begin{bmatrix} {}^{S \rightarrow P} \mathbf{g} \end{bmatrix} \quad (6.2)$$

6.4 Discretization scheme

A tessellation scheme of ten degrees for orientation space and three degrees for θ intervals was used for this project. The fundamental zone for hexagonal close pack materials such as α -titanium, as illustrated in Figure (6.2), is defined with Bunge – Euler angles in Euler space as $\varphi_1 \in (0, 2\pi), \Phi \in (0, \pi/2), \varphi_2 \in (0, \pi/3)$ [21]. Additionally, the grain size interval was incremented by a distance of 1 μm between adjacent centroids.

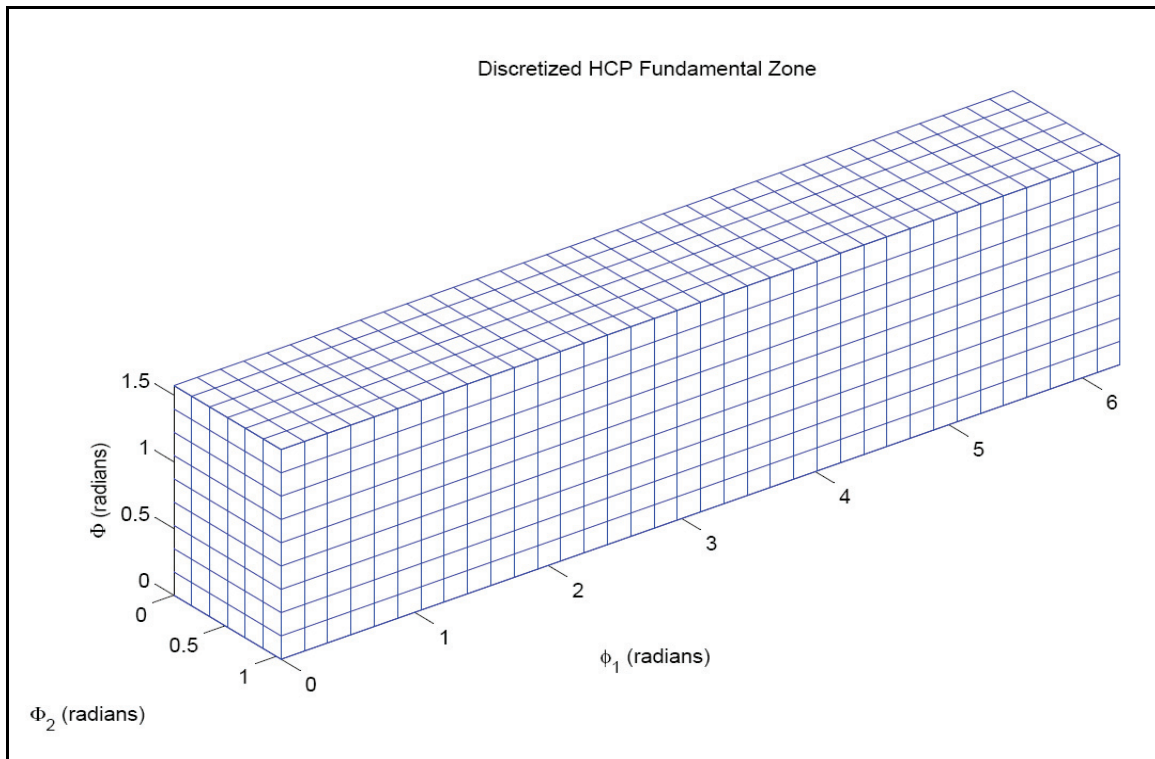


Figure 6.1: Discretized HCP fundamental zone shown for 10 degree bin sizes

7 Discussion of Results

7.1 Deviatoric stress subspace

Figure 7.1 represents one of numerous combinations of deviatoric stress subspaces that can be extracted from the full five dimensional deviatoric stress space and illustrated as a three dimensional object. In this case, σ'_{11} , σ'_{22} , and σ'_{12} were selected and the other two values of stress, σ'_{23} , and σ'_{13} , were allowed to vary over all possible values. However, any three of the five stresses could have been selected here.

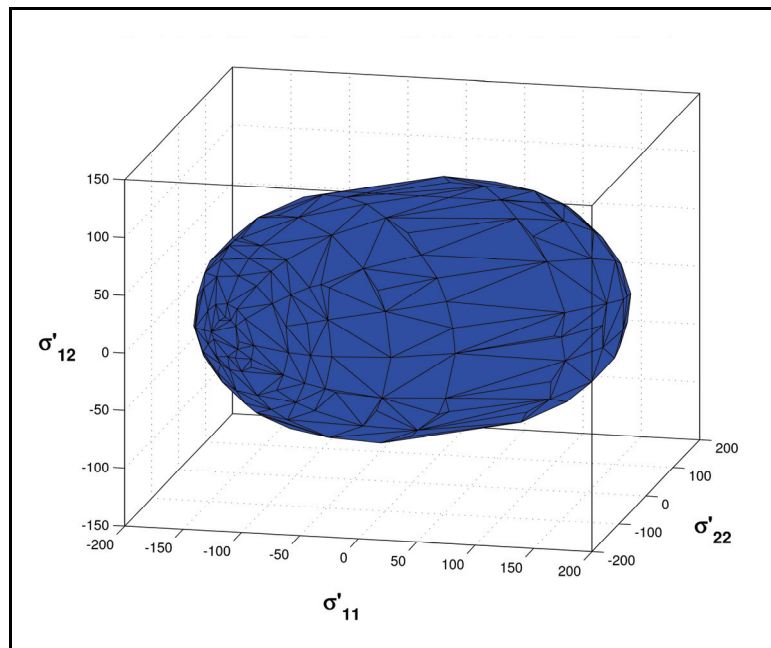


Figure 7.1: Deviatoric stress subspace plot for high purity α -titanium (all units are in MPa)

7.2 Yield surface plots

Yield surface plots were chosen as a convenient way to visually compare the results found in this paper. The yield loci in Figure 7.2 represents yield surfaces in the π -plane for the α -titanium material. Using the definition for the rate of plastic work, \dot{W}_p , as expressed in Equation (7.1), we have chosen to normalize the stresses plotted in each yield surfaces such that the rate of plastic work is constant for each point on the yield surface. A value of 3.52 MPa/s was enforced for each point; it represents the value resulting from the simple case of uniaxial compression in the ND direction.

$$\dot{W}_p = \sum_{i=1}^3 \sum_{j=1}^3 \sigma'_{ij} \dot{\epsilon}_{ij} \quad (7.1)$$

The red surface in Figure 7.2 represents the Von-Mises or isotropic case, the blue curve corresponds to the new grain size adjusted Taylor model, the green curve represents the traditional Taylor viscoplastic solution, and the black triangles show the experimentally obtained yield points. It is observable that the traditional method, which only accounts for variations in texture, accurately predicts the yield surface in the σ'_{11} and σ'_{22} directions but substantially underestimates the yield surface in the σ'_{33} direction of the material. The new grain size differentiated model on the other hand slightly over-predicts the yield surface in the σ'_{11} and σ'_{22} direction but does a reasonable job in predicting the anisotropic yield response of the material in the σ'_{33} direction. The empty regions between the two Taylor models of Figure 7.2 substantiate the idea that a material's grain size distribution contributes significantly to its yield strength. We would expect this effect to be even more pronounced for materials with a large Hall-Petch slope,

materials with large grain size variations, partially recrystallized textures, or materials with elongated grain structures.

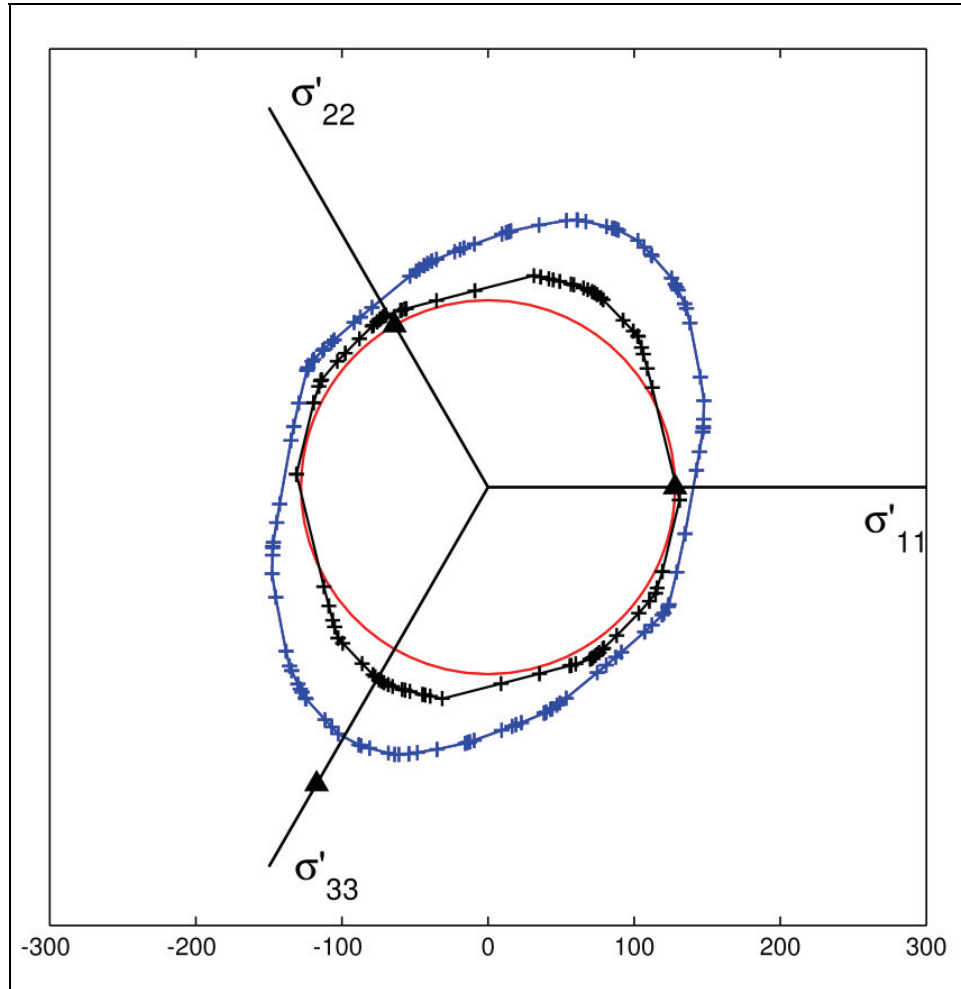


Figure 7.2: Pi-section yield surface comparing Von-Mises yield surface in red, traditional Taylor model in black, and the new grain size dependent model in blue (all units are in MPa)

7.3 Effect of numerical methods on yield surfaces

The coarseness of the discretized bins had a noticeable effect on the yield surface calculations. Several studies were conducted to determine what parameters affected the yield loci. It was found that grain size binning had the biggest effect. Figure 7.3 shows

yield surfaces for the following three cases: 1 grain size bin (black), 10 grain size bins (green), and 40 grain size bins (blue). The yield surface was underestimated for the case with only one grain size bin and was overestimated for the case with 10 grain size bins. In order to avoid numerical effects, it is necessary to utilize sufficient grain size bins to accommodate the grain size distribution of the material.

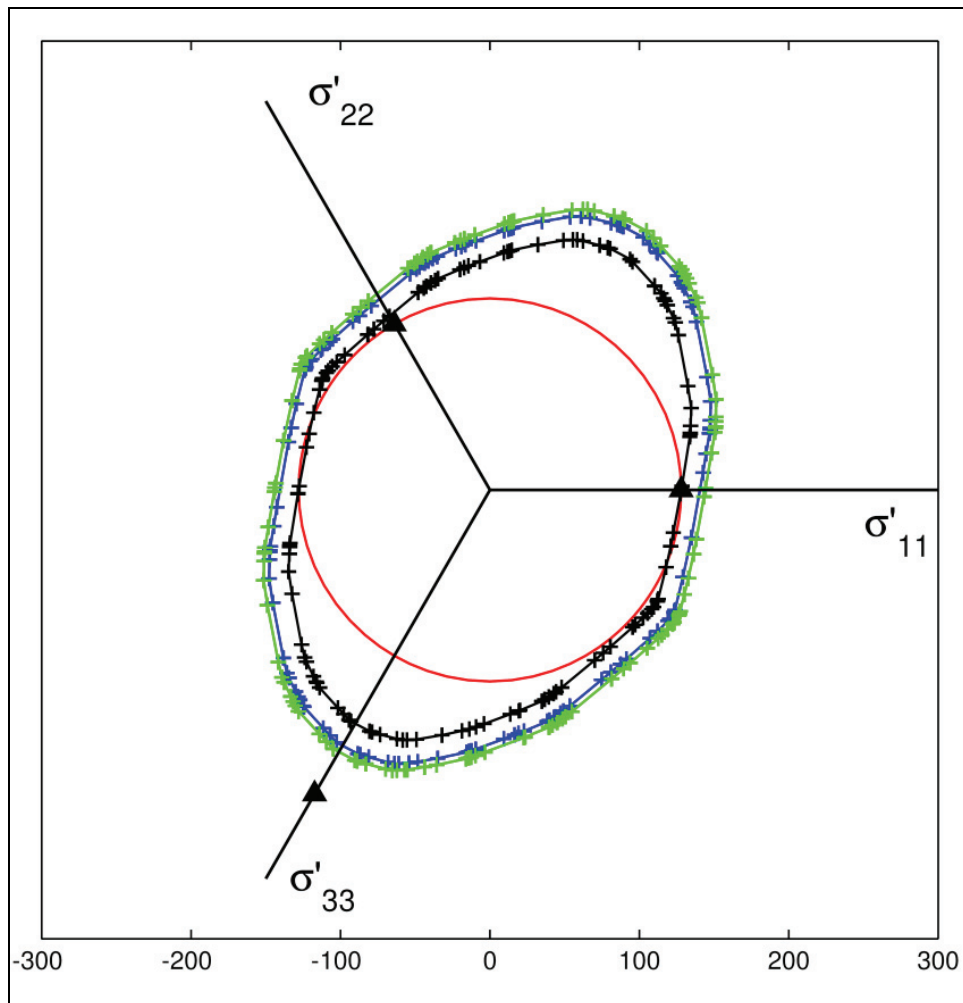


Figure 7.3: Effect of grain size bins on size of yield surface where the black curve was calculated with a single grain size bin, the green curve incremented grains size into 10 segments, and the blue curve represents the curve calculated with 40 grain size bins (all units are MPa)

A second effect worth mentioning is the difference in yield surface shape caused by varying the number of points sampled to create the yield surface. Figure 7.4 compares three yield surfaces: (a) 768 points in black, (b) 1,500 points in green, and (c) 4,500 points plotted in blue. A minimum of 1,500 points is recommended to ensure a uniformly sampled yield surface.

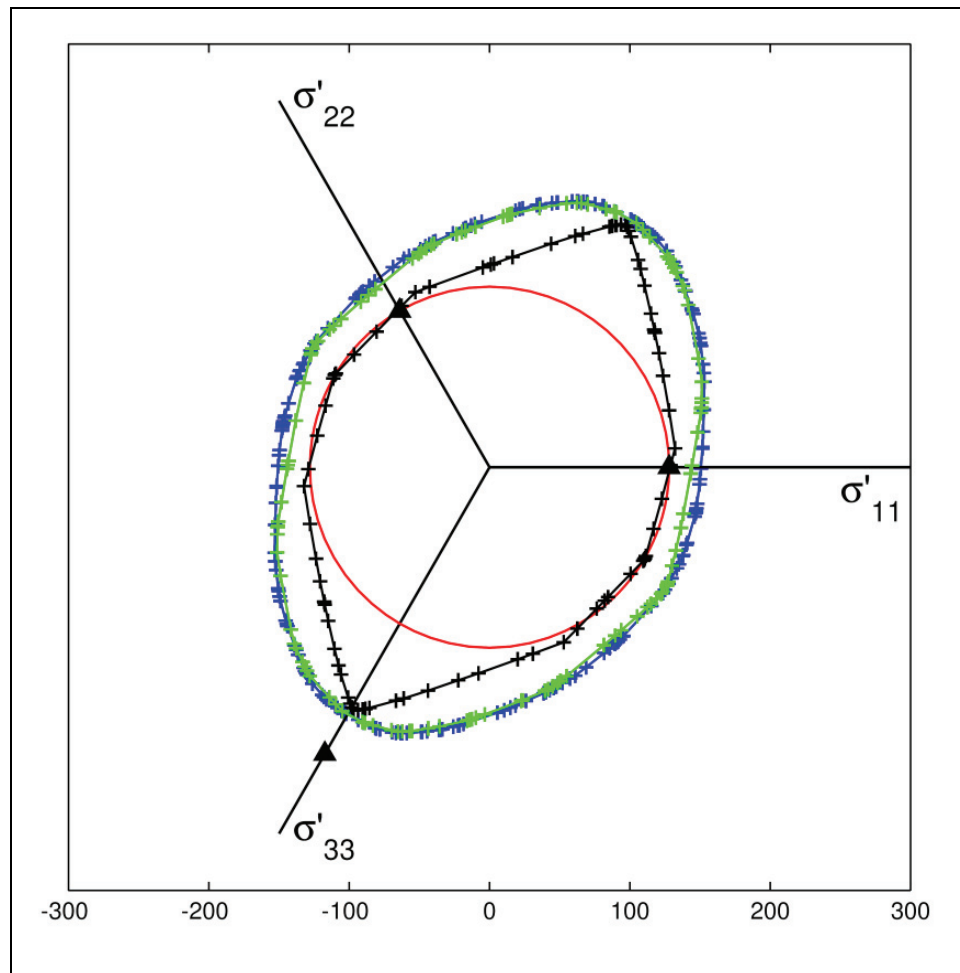


Figure 7.4: Effect of number of yield points on yield surface. The black curve was calculated using 768 points, the green with 1,500 points, and the blue curve with 4,500 individual points (all units are in MPa)

8 Conclusions

The goal of this work has been to introduce a new methodology whereby the grain size distribution can be introduced into crystal plasticity. A new distribution function, similar to the orientation distribution function, but adjusted for grain size, has been defined. This new grain size and orientation distribution function can be recovered through orientation imaging microscopy that simultaneously recovers the chord length distribution. The methodology has been demonstrated for a high purity sample of α -titanium. Experimental methods used to calibrate the new model were described and results were presented as yield surfaces in deviatoric stress space. The following conclusions and observations can be drawn from this study:

- Grain size and its distribution have a significant impact on the yielding characteristics of α -titanium, in that both the size and shape of the yield surface were affected
- The chord length distribution is an effective tool in recovering grain size statistics
- A mesoscale Hall-Petch relationship can be successfully incorporated into Taylor viscoplasticity
- Introducing grain size as a variable in Taylor viscoplasticity more accurately predicts the anisotropic yield loci of hexagonal close pack α -titanium as compared to the traditional approach

References

- [1] Petch NJ, The Cleavage Strength of Polycrystals, *Journal of the Iron and Steel Institute*, vol. 174 ,1953, pp. 25-28.
- [2] Hall EO, The Deformation and Ageing of Mild Steel: III Discussion of Results, *Proceedings of the Physical Society of London*, vol. B64, 1951, pp. 747-753.
- [3] Masumura RA, Hazzledine PM, and Pande CS, Yield stress of fine grained materials. *Acta Materialia*, vol. 46, 1998, pp. 4527-4534.
- [4] Schiotz J, Jacobsen KW, A maximum in the strength of nanocrystalline copper, *Science*, vol. 301, 2003, pp. 1357-1359.
- [5] Taylor GI, Plastic Strain in Metals, *Journal of the Institute of Metals*, vol. 62, 1938, pp. 307-324.
- [6] Salem AA, Kalidindi SR, and Doherty RD, Strain hardening regimes and microstructure evolution during large strain compression of high purity titanium, *Scripta Materialia*, vol. 46, 2002, pp. 419-423.
- [7] Salem AA, Kalidindi SR, Doherty RD and Semiatin SL, Strain Hardening Due to Deformation Twinning in α -Ti: Mechanisms, *Metallurgical and Materials Transactions A*, vol. 37A, 2006, pp. 259-268.
- [8] Bata V and Pereloma E, An alternate explanation of the Hall-Petch relation, *Acta Materialia*, vol. 52, 2004, p. 657-665.
- [9] Soer WA, Aifantis KE, and De Hosson JTM, Incipient plasticity during nanoindentation at grain boundaries in body-centered cubic metals, *Acta Materialia*, vol. 53, 2005, pp. 4665-4676.
- [10] Asaro RJ, Needleman A, Texture development and strain hardening in rate dependent polycrystals, *Acta Materialia*, vol. 33, 1985, p. 923.
- [11] Salem AA, Kalidindi SR, Semiatin SL, Strain hardening due to deformation twinning in α -titanium: Constitutive relations and crystal-plasticity modeling, *Acta Materialia*, vol. 53, 2005, pp. 3495-3502.

- [12] Kalidindi SR, Duvvuru HK, Spectral methods for capturing crystallographic texture evolution during large plastic strains in metals, *Acta Materialia*, vol. 53, 2005, pp. 3613-3623.
- [13] Wu XP, Kalidindi SR, Necker C, Salem AA, Prediction of Crystallographic texture evolution and anisotropic stress-strain curves during large plastic strains in high purity α -titanium using a Taylor-type crystal plasticity model, *Acta Materialia*, Vol.55, 2007, pp. 423-432.
- [14] Knezevic M., Kalidindi SR, Fullwood D, Computationally efficient database and spectral interpolation for fully plastic Taylor-type crystal plasticity calculations of face-centered cubic polycrystals, *International Journal of Plasticity*, (accepted).
- [15] Hutchinson JW, Bounds and self-consistent estimates for creep of polycrystalline materials, *Proceedings of the Royal Society of London*, vol. 348, 1976, pp. 101-126.
- [16] Matheron G, Random Sets and Integral Geometry, *Wiley & Sons*, New York, 1975.
- [17] Torquato S and Lu B, Chord length distribution function for two-phase random media, *Physical Review E.*, vol. 47, 1993, pp. 2950-2953.
- [18] Salem AA, Kalidindi SR, Doherty RD, Strain hardening of titanium: role of deformation twinning, *Acta Materialia*, vol. 51, 2003, pp. 4225-4237.
- [19] Hilliard JE, Lawson LR, Stereology and Stochastic Geometry, *Kluwer Academic Publishers*, Boston, 2003.
- [20] Churchman AT, The Slip Modes of Titanium and the Effect of Purity on their Occurrence during Tensile Deformation of Single Crystals, *Proceedings of the Royal Society of London. Series A, Mathematical and Physical Sciences*, vol. 226, No. 1165, 1954, pp. 216-226.
- [21] Bunge HJ, Texture analysis in materials science, Mathematical methods, *Cuvillier*, Gottingen, 1993.